SAND2017-13127C

USING TEMPORAL MOMENTS TO DETECT INTERACTIONS DURING SIMULTANEOUS SHOCK TESTING OF MULTIPLE COMPONENTS

Carl Sisemore, Vit Babuška, Jason Booher
Sandia National Laboratories[1]
Albuquerque, NM 87185

ABSTRACT

Small components are often tested in groups with several components mounted to a common test fixture and tested simultaneously. This test method is frequently used to reduce the time spent in the test laboratory. There is an inherent problem testing multiple identical components simultaneously since the overall fixture-component system will possess a number of closely spaced vibration modes. This is a direct result of the components all having nearly identical mass and stiffness. The ramifications of this is that the shock applied to the fixture may not be evenly distributed to all components, resulting in some being tested more severely than others. This is possible even with a well-designed fixture. This paper presents a novel application of temporal moments for detecting and quantifying the interaction between multiple components from a single shock test. The paper also presents a series of experimental results showing how the temporal moments shift as damage progresses through the multi-component system.

INTRODUCTION

Simultaneous testing of multiple components is a common method to reduce test time in the laboratory. If components are small enough, it is frequently possible to test two or more units on the same test fixture. This can result in dramatic reductions in the amount of time spent testing, especially if large numbers of parts are required to undergo the same testing schedule. However, there is an inherent problem with this type of testing since the various components will interact with one another in some manner. The reason for this is well understood. If two nominally identical components are mounted to the same test fixture, then the fixture-component system inherently has a series of closely-spaced modes. It is also readily apparent that the two nominally identical components being tested will not have identically equivalent modes or frequencies simply due to variations in manufacturing tolerances. As the various components under test interact with each other, it is possible to create situations in which one component is exposed to higher test levels than another.

Closely-spaced modes are defined as vibration modes with frequencies close to a common mean. Typically, modes are considered to be closely-spaced when they are within about ten percent of the mean. They can become especially problematic when their modal effective masses are significant and approximately the same order of magnitude [1]. With simultaneous testing of multiple components, the modal masses are, by definition, the same order of magnitude. If the units under test are installed on a small test fixture, they can also become a significant portion of the total modal mass. This is the definition for creating a significant problem, not the definition for creating influence. This work shows that even when the modal mass is not a significant portion of the total system mass, the influence of closely-spaced modes can be detected.

Temporal moments were proposed by Smallwood [2, 3] to augment shock specification information. While the Shock Response Spectra (SRS) is typically used to define a shock test, a significant disadvantage of the SRS is that all temporal information about the transient is lost. Since the SRS transform significantly reduces the quantity of data preserved about the shock transient, it is in turn possible to create many transient shock events that result in the same SRS. Thus, temporal moments were proposed as a way to help distinguish between two time histories that yield

[1] Sandia National Laboratories is a multimission laboratory managed and operated by National Technology and Engineering Solutions of Sandia, LLC., a wholly owned subsidiary of Honeywell International, Inc., for the U.S. Department of Energy's National Nuclear Security Administration under contract DE-NA0003525.

nominally identical SRS curves. In the same way, it should be possible to analyze data from two nominally identical shock time histories to see if the temporal moments can discriminate between the event severities.

The work described in this paper is the result of numerous experimental cases where multiple cantilever beams were tested simultaneously. Simultaneous testing was done for the obvious reason of increasing the number of tests to failure that could be accomplished in the limited time available. While testing was being performed it begin to appear that the failure results were not entirely random as would have been expected. Rather it seemed that there were interactions between the different test specimen. As a result, several methods were investigated to see if it would be possible to discern and quantify the nature of the interaction between components. Applying temporal moments to the data collected provided a level of discrimination between component responses that helped to explain the laboratory results.

OVERVIEW OF TEMPORAL MOMENTS

The fundamental problem with the SRS is that a field event might be more easily replicated in the laboratory with a significantly different transient that yields the correct SRS but may not excite the same modal response of the test article. This in turn could easily lead to successful laboratory testing and field failures. Temporal moments were derived as a way to reduce the time signal information to a few quantities of interest that would supplement the SRS when defining shock test specifications.

The i[th] temporal moment, $m_i(a)$, of a time history, $x(t)$, about a time, a, was defined by Smallwood as:

$$m_i(a) = \int_{-\infty}^{\infty} (t-a)^i [x(t)]^2 dt. \tag{1}$$

The temporal moment equation was defined analogously to the equations for probability moments; however, the two are fundamentally different in that probability moments operate on a probability distribution function whereas temporal moments operate on a time history. The temporal moments are actually defined in terms of the square of the time history. This was done partly as a matter of convenience to ensure that the first temporal moment was a positive value greater than zero. Calculating the area under the raw shock time history curve will frequently yield a result close to zero. The other reason for using the square of the time history is that Parseval's theorem states that the integral of the time history squared and the integral of the Fourier transform squared both give a measure of signal power.

The zero order temporal moment, m_0, is independent of the time shift, a, as seen from Equation 1. The zero order moment is usually referred to as the energy, E, although the units are actually power per unit mass. However, for the sake of consistency, the zeroth order moment will be referred to as the energy throughout this paper.

The first order temporal moment, m_1, normalized by the energy gives the signal centroid. This is the time where the centroid of the energy is located. Because the origin of the time axis is frequently arbitrary, calculating the higher order temporal moments about the centroid helps to provide consistency between comparisons. To calculate the centroid, the first order moment is given by the expression

$$m_1(a) = \int_{-\infty}^{\infty} (t-a)[x(t)]^2 dt. \tag{2}$$

To normalize Equation 2, the first order moment is defined to be zero and the offset is calculated.

$$m_1(a) = \int_{-\infty}^{\infty} t[x(t)]^2 dt - a\int_{-\infty}^{\infty} [x(t)]^2 dt = 0. \tag{3}$$

The offset, a, to the centroid is usually given the designation τ in the literature and is obtained from rearranging Equation 3 as

$$a = \tau = \frac{\int_{-\infty}^{\infty} t[x(t)]^2 dt}{\int_{-\infty}^{\infty} [x(t)]^2 dt} = \frac{\int_{-\infty}^{\infty} t[x(t)]^2 dt}{m_0}. \quad (4)$$

The signal centroid varies with the choice of the time origin. For this reason, the higher order temporal moments are calculated about the centroid rather than about time axis origin. The zeroth order moment is independent of the time axis origin so it is unchanged.

The second order temporal moment, m_2, normalized by the energy is defined as the mean square duration of the time history. The square root of this value is known as the RMS duration. This value is often used to define the duration of a complex signal and provides criterion to evaluate the length of a laboratory shock event against the length of a field measured shock event. The RMS duration is given by the equation:

c

$$D_\tau = \sqrt{\frac{m_2(\tau)}{m_0}} = \sqrt{\frac{\int_{-\infty}^{\infty} (t-\tau)^2 [x(t)]^2 dt}{m_0}}. \quad (5)$$

It should be noted that the RMS duration does not represent the actual duration of the transient shock time history. Rather, it is supposed to define a time window centered about the centroid of the shock signal where the most significant portion of the shock transient occurs.

The third and fourth order normalized temporal moments are known as the skewness and kurtosis, respectively. They can be derived from Equation 1 by the expression

$$S_\tau = \sqrt[3]{m_3(\tau)/m_0} \quad (6)$$

for the skewness, and the kurtosis by

$$K_\tau = \sqrt[4]{m_4(\tau)/m_0}. \quad (7)$$

Calculation of the temporal moments is straightforward using numerical integration of the time history signal. However, one of the fundamental concerns with using temporal moments on experimental data is the effect of signal noise. The above integral relations are clearly defined for classical analytical shock pulses and temporal moments directly calculated for simple pulses such as a haversine or half-sine shock. Classical shock pulses also decay to zero and remain there. In contrast, experimentally obtained data decays to a noise floor which can cause some difficulties when calculating temporal moments.

TEMPORAL MOMENTS FROM EXPERIMENTAL DATA

Calculation of temporal moments using experimentally measured shock data is done frequently. However, as was stated previously, there is a risk with this approach since measured shock test data decays to the noise floor and not to zero as is the case with an ideal, classical shock pulse. It has been stated previously that there is a need to use caution when calculating temporal moments on experimental data, but this has not been well quantified.

Figure 1 shows a plot of a typical low acceleration time history input recorded on a drop table. This time history is one that could be reasonably used for calculating temporal moments. The signal includes some pre-trigger data, the shock nominally peaks around time $t = 0$, and some post-event data are captured to ensure the response is completely characterized.

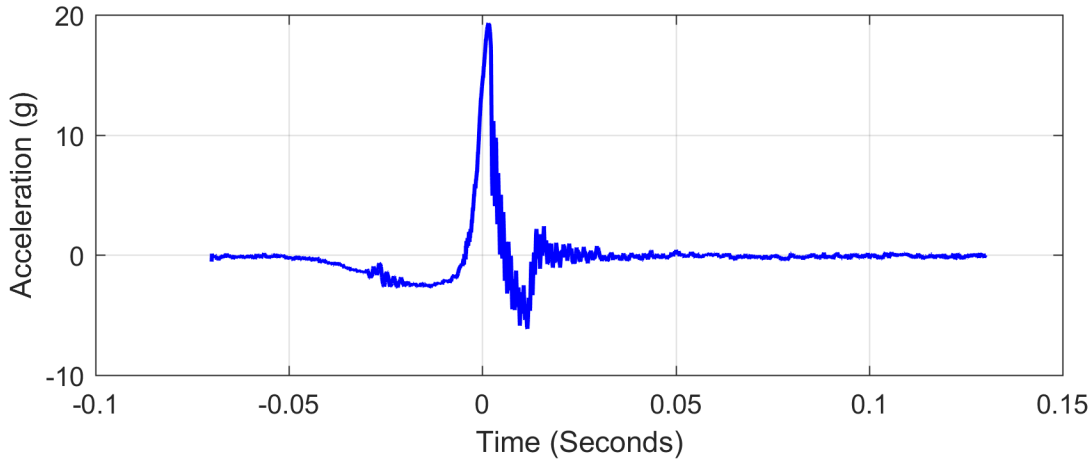

Figure 1. Measured Acceleration Time History from Drop Table Testing

Normally, temporal moments are calculated as scalar values. The integration is performed and a single number returned. However, it is insightful to calculate and plot the temporal moments as a function of time. Figure 2 shows a plot of the zeroth temporal moment (energy) with respect to time for the drop table shock shown in Figure 1. The energy starts near zero, rises slightly with the motion before the primary impact, rises sharply with the shock impact and trends to a flat line as the shock decays to zero as expected. However, the inset plot in Figure 2 gives a slightly different result. The inset plot shows that the energy actually increases post-shock all the way to the end of the time history. The reason is that the noise floor from about 0.03 seconds out to the end of the record is included in the calculation. From Equation 1, the noise floor is squared so the signal is always positive and continues to add to the overall measured energy. In this example, the energy at the record end is only about 0.2 percent greater than the energy at 0.03 seconds—certainly a minor difference.

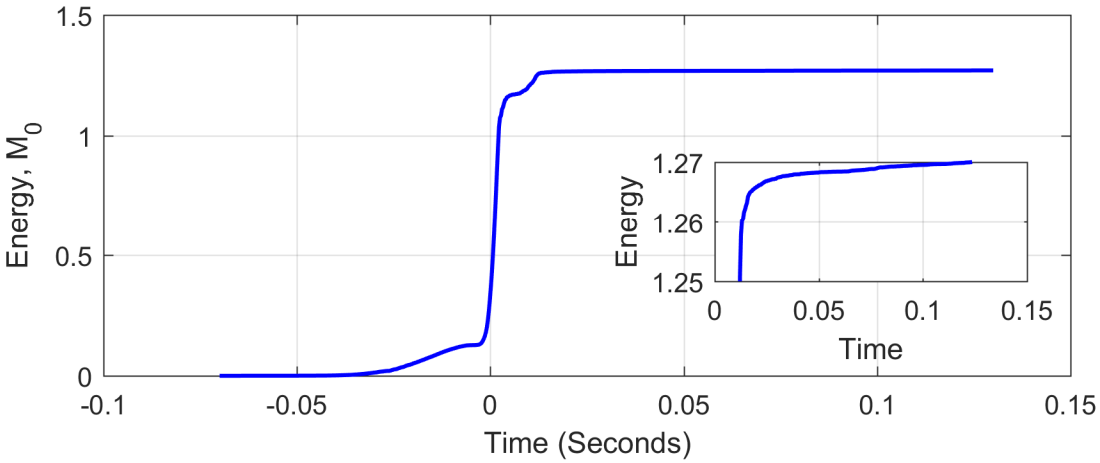

Figure 2. Energy Calculated from Measured Drop Table Data

Figure 3 shows a similar trend with the shock centroid. The centroid represents the point where approximately half of the energy occurs before the centroid time and half after the centroid time. From the time history plot shown in Figure 1, this point is intuitively about zero since the primary shock pulse was centered at about $t = 0$. The plot shows the centroid goes to approximately zero post-shock, as would be expected. However, here again the inset plot shows a shallow but steady rise in the centroid result post-shock. The percent error here is large but not particularly significant because the actual numbers are so close to zero.

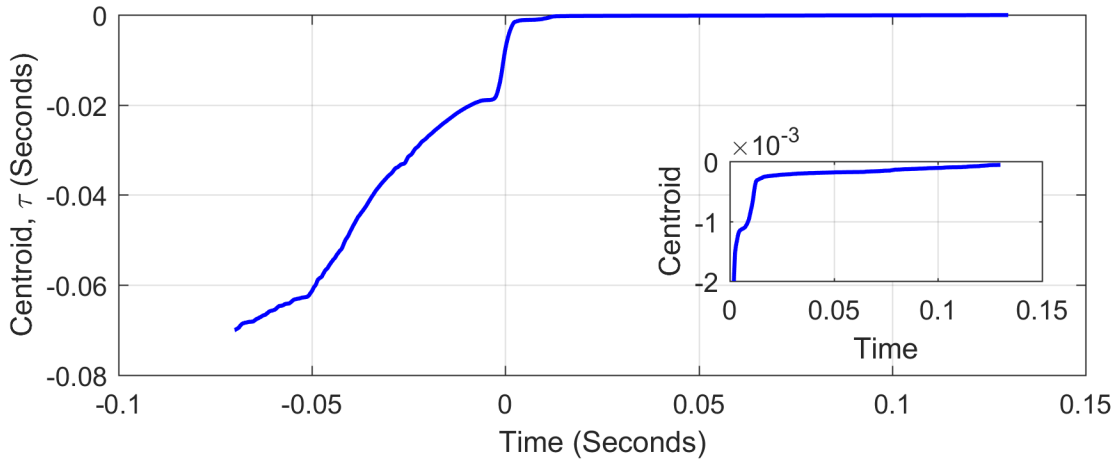

Figure 3. Shock Centroid from Measured Drop Table Data

Figure 4 shows the RMS duration calculated from the time history plot shown in Figure 1. With these data, the instability in the RMS duration is obvious. The RMS duration that would normally be obtained from a numerical integration of Equation 1 is the value at the end of the record which is not asymptotically trending to a fixed value, neither is it the maximum value measured during the record. The difference here is 11 percent between the RMS duration at 0.03 seconds and the RMS duration at the end. The difference is 45 percent between the maximum RMS duration from Figure 4 and the RMS duration at 0.03 seconds. Since the RMS duration is frequently proposed as a measure of the shock event duration in test specifications, it is easy to see how the difference seen here could become significant.

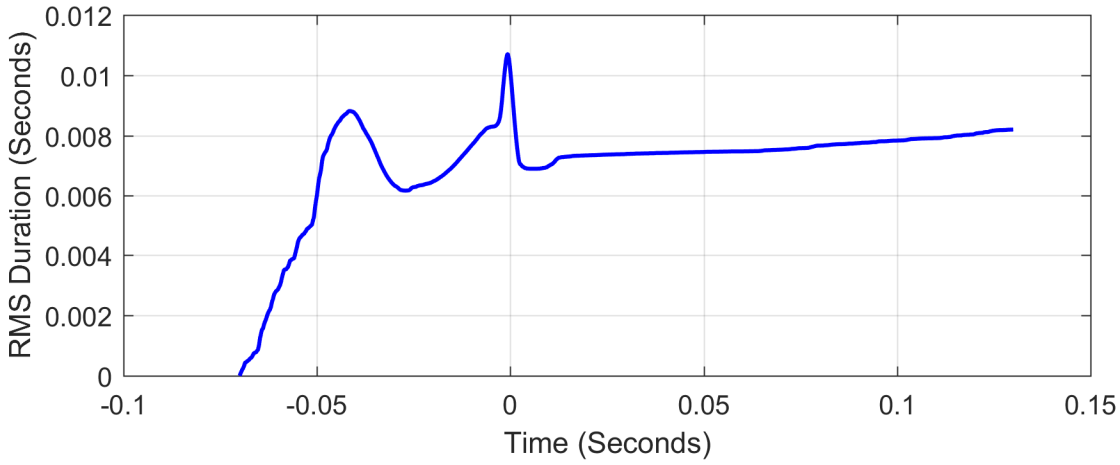

Figure 4. Shock RMS Duration from Measured Drop Table Data

The skewness of a classical haversine shock should be zero since the haversine shock is symmetric about the shock centroid. An experimentally measured drop shock is a good approximation to a haversine but not necessarily exact so some deviation from the expected value is not unreasonable. However, Figure 5 shows a plot of the skewness change as a function of time for the drop shock time history of Figure 1. While the overall value is low, agreeing with the zero skewness of a classical haversine, the fluctuations are dramatic. The sharp decrease at -0.05 seconds and increase at 0.122 seconds are the results of sign changes in the skewness.

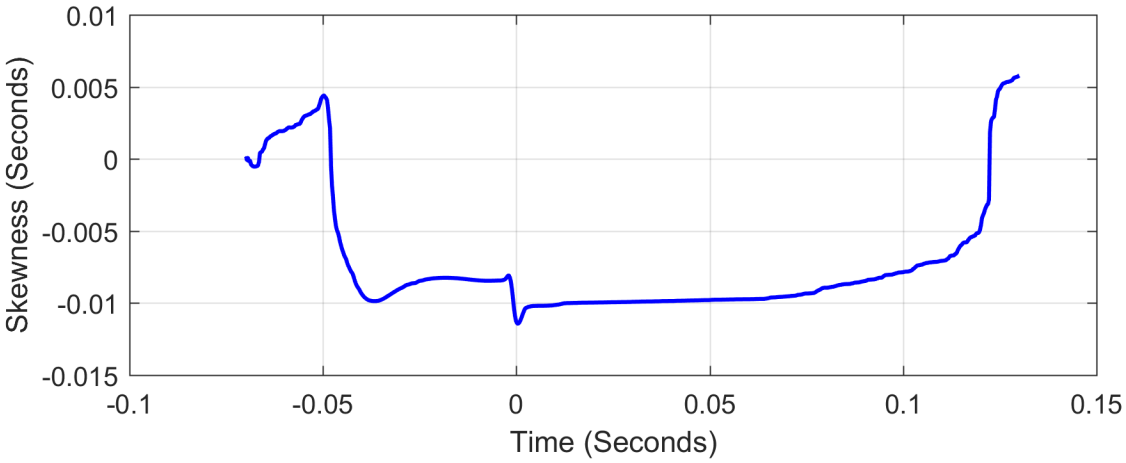

Figure 5. Shock Skewness from Measured Drop Table Data

Kurtosis is a measure of infrequent extreme deviations in a distribution. Figure 6 shows a plot of the measured data kurtosis as a function of time from the drop shock shown in Figure 1. It can be seen that the kurtosis starts to dramatically increase post-shock. There is a 45 percent increase in the kurtosis value from the value at 0.03 seconds to the end value. The reason for this is that as more noise is included in the signal, the noise trends to the mean and the single shock excursion becomes more of an outlier in the data, hence the increasing kurtosis.

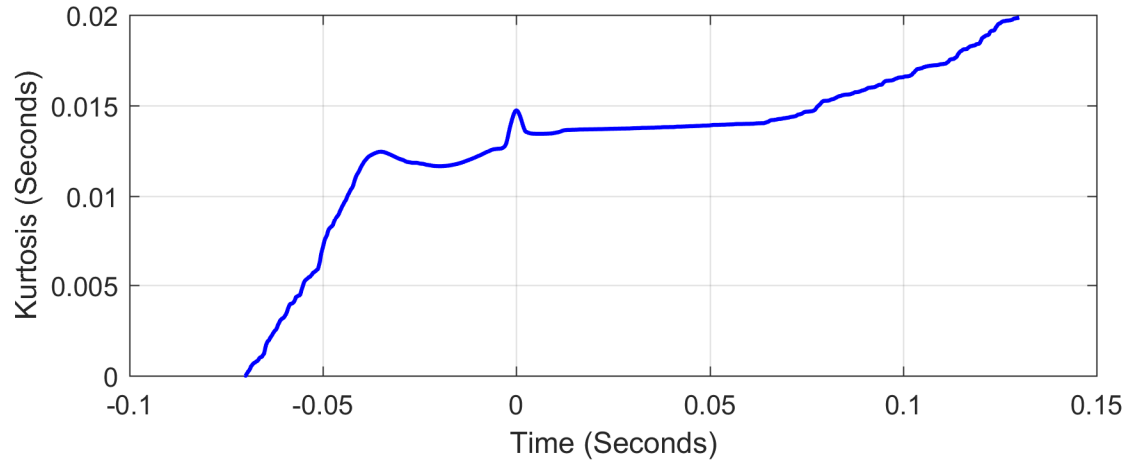

Figure 6. Shock Kurtosis from Measured Drop Table Data

Based on the above results, it would be reasonable to return to the time history plot and truncate the shock signal at about 0.03 seconds when calculating the temporal moments. This result is based solely on inspection of the data, considering the points where the time history appears to decay to the noise floor. This is somewhat different from the inflection points in the energy and RMS duration plots but it is similar.

The El Centro, California 18 May 1940 earthquake response provides another interesting example. Figure 7 shows a plot of the time history from the North-South response. It is assumed that none of the data have actually returned to the noise floor, even at the end of the record since the level there is about 0.01g. However, the time history data indicate two likely locations for cropping the signal: first at about 26.5 seconds and finally at the record end which is apparently where the original archivers of the data believed it should be truncated or where they ran out of recorded signal. Figure 8 shows a plot of the energy versus time calculated using temporal moments. From this plot there is a

relatively minor 3.5 percent difference between the energy at 26.5 seconds and the energy at the record end, 53.7 seconds. Figure 9 shows a plot of the RMS duration. Here there is a 16 percent increase in the RMS duration from 7.42 seconds RMS duration if the response is cropped at 26.5 seconds up to 8.64 seconds RMS duration if the entire record length is used.

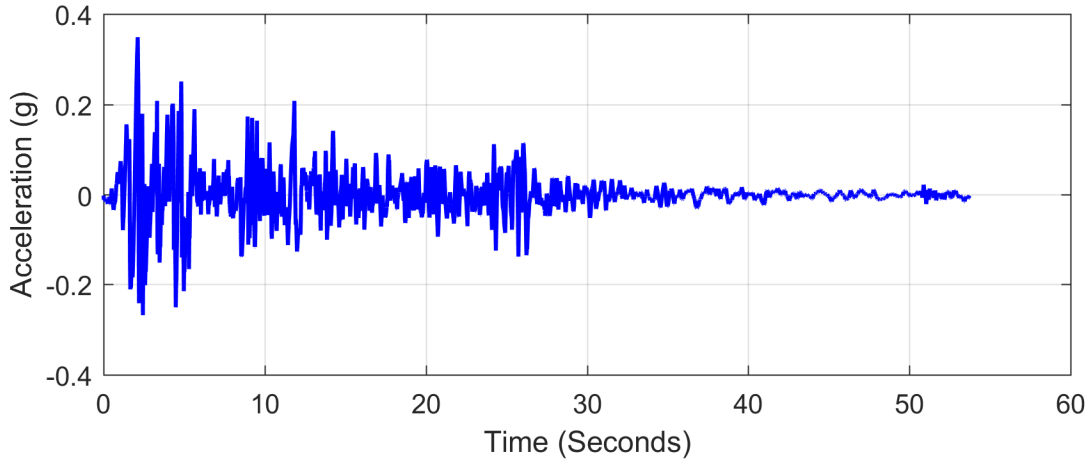

Figure 7. El Centro North-South 18 May 1940 Earthquake Acceleration Time History

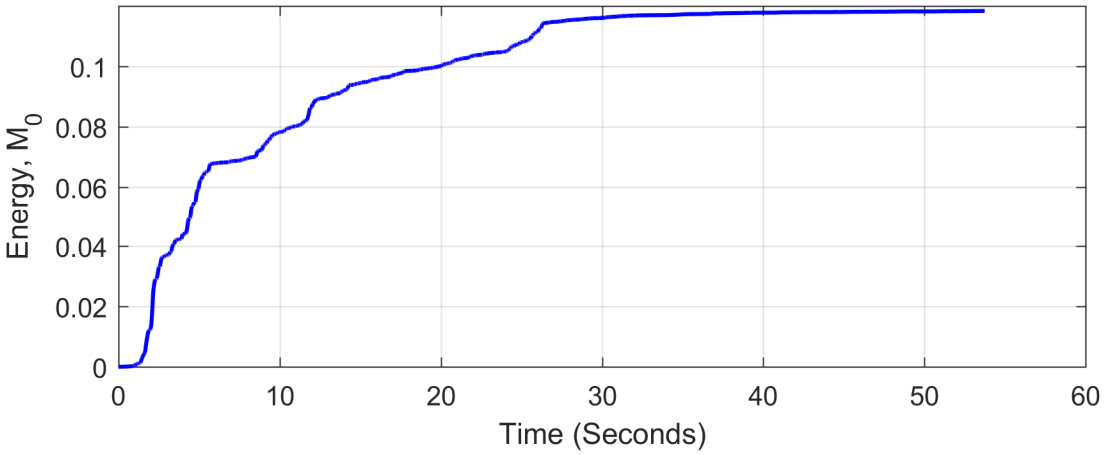

Figure 8. El Centro North-South Energy

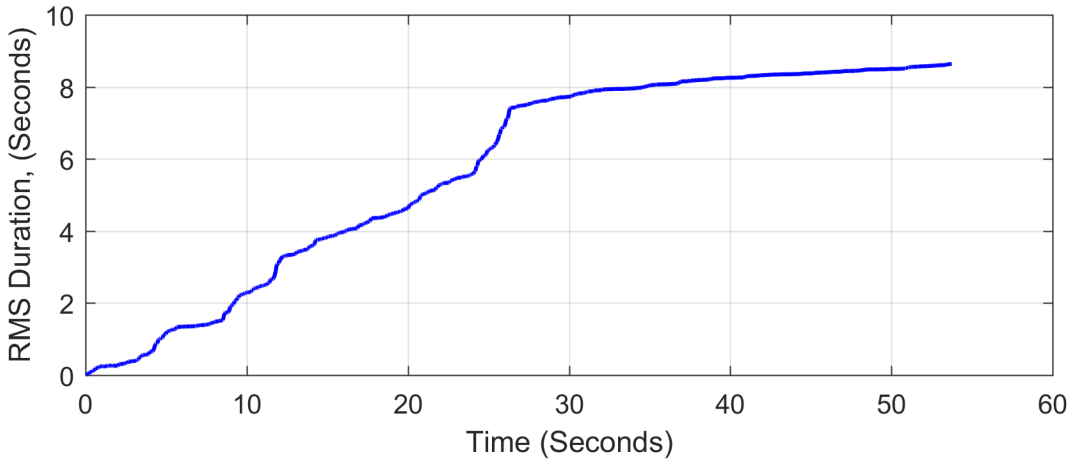

Figure 9. El Centro North-South RMS Duration

Based on the data presented here, one of two options for trimming a shock time history is required for proper characterization by temporal moments. The first, and perhaps the best option is to truncate the shock time history at the point that the signal reaches the noise floor and then note this signal duration along with the RMS duration. The second option is to use a fixed signal length for all calculations. This second option may be preferable when many similar shocks are to be analyzed using the same equipment and analysis methodologies.

SHOCK TESTING OVERVIEW

The experimental portion of this study made use of 3D printed cantilever beams tested in the Sandia National Laboratories Component Dynamics Laboratory on a small modal shaker system. The cantilever beams used for this investigation were made from ABS plastic and printed by the Sandia National Laboratories Additive Manufacturing group. A photograph of the test setup is shown in Figure 10. The tests were conducted in sets of four beams and a repetitive shock load was applied until all four beams failed. Since a relatively small shaker was used, a gravity off-load system was incorporated using soft springs to support the test fixture's weight independent of the shaker armature. This allowed for higher acceleration loads to be used for these experiments. Figure 11 shows a photograph of this gravity off-load system.

Figure 12 shows a close-up photograph of one cantilever beam used for testing. The beams were five inches long and 0.25 inches in diameter. All of the beams had a 0.025inch notch near the base to create a stress concentration point. This feature helped ensure that all the beams failed at the same location. A steel collar with an attached accelerometer was added at the free end to measure the response but also to increase the bending moment in the beam. The added weight at the cantilever beam free end was about 0.0289 lbf (13.1grams).

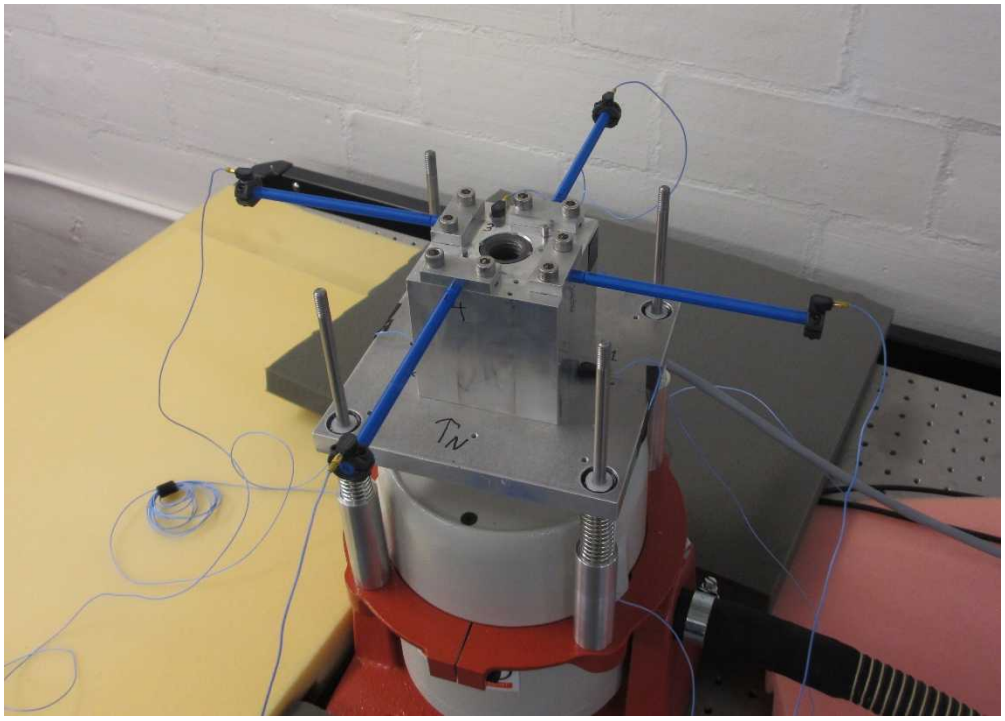

Figure 10. Shaker Test Setup with Four Cantilever Beams Installed

Figure 11. Shaker Test Setup Showing Gravity Off-Load Configuration

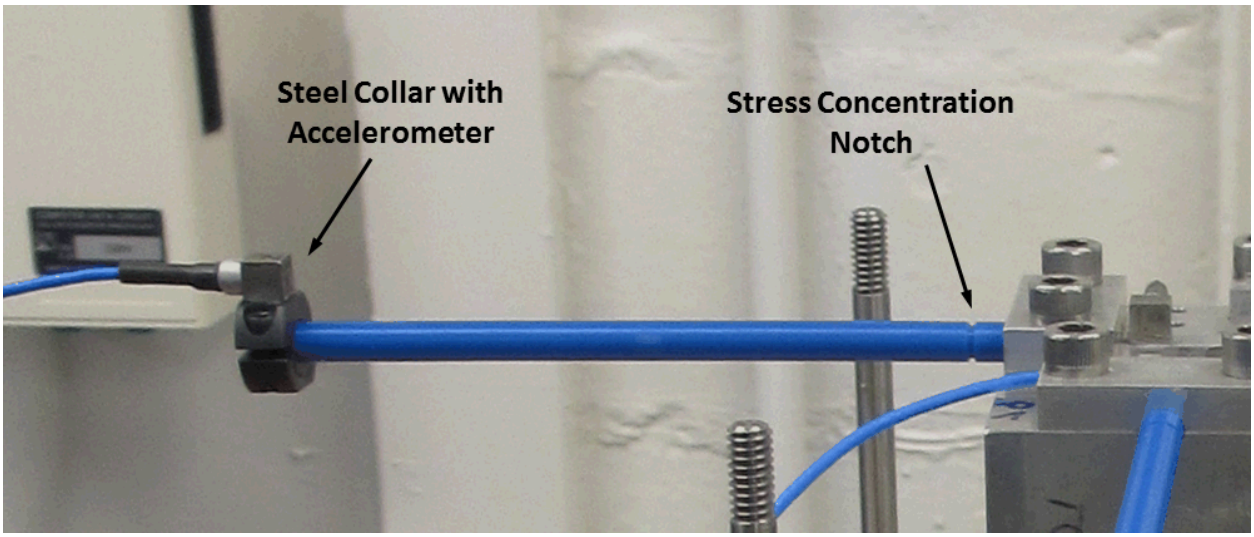

Figure 12. Cantilever Beam Test Specimen Showing Stress Concentration and Tip Weight

The fundamental natural frequency of the test fixture is defined by the modes of the aluminum plate to which the tower holding the cantilever beams is attached. The first mode of the 0.50inch aluminum plate is 1350Hz per the equations for a free-free plate from Blevins [4]. The fundamental natural frequency of the cantilever beams was measured at about 23Hz. Since there is a factor of 50 difference between the fundamental mode of the fixture and the fundamental mode of the test articles, one would not expect any measurable interaction between components in this multi-component test configuration.

SHOCK TEST RESULTS

Figure 13 shows a plot of a typical shock time history used for these tests. This same shock was repeated until all the beam specimen failed. Figure 14 shows an overlay plot of the measured responses to the shock input at the free ends of the four cantilever beams. As expected from a cantilever beam, the response is heavily dominated by the beam's first natural frequency, about 24 Hz in this example. A careful examination of Figure 14 does show that while all the beams start out moving together, they begin to oscillate out of phase with each other relatively quickly. By the time the response has nearly damped out, the beams opposite one another, North-South and East-West, are almost completely out of phase with each other. Figure 15 shows a comparison of the pseudo-velocity Shock Response Spectra (SRS) for this shock calculated from the beam's free-end response. As can be seen here, the SRS from all four beams are essentially identical with only minor deviations.

The shock test was repeated using the same shaker shock until all four beams failed. Failure was defined as a complete fracture of the beam such that the beam fell off the test fixture. At that point, the failed beam was removed and testing continued with one fewer beam in place.

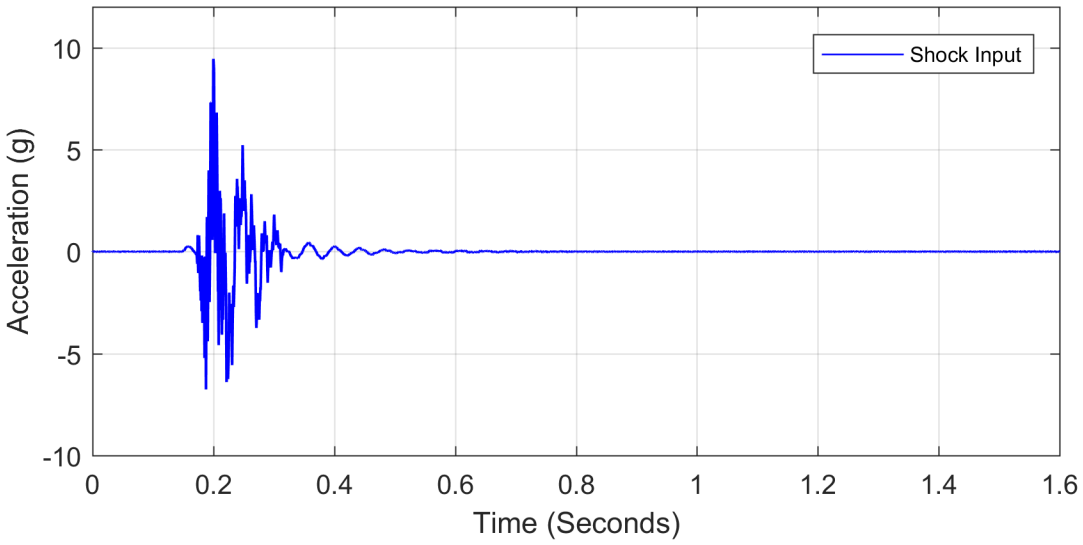

Figure 13. Typical Shaker Shock Base Excitation Time History

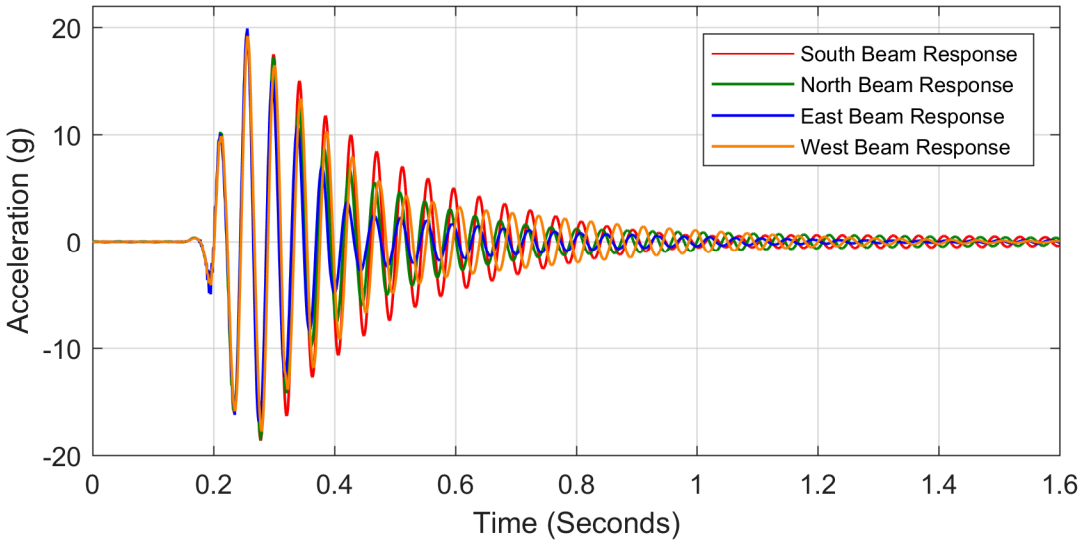

Figure 14. Response at Four Beam Tips—Shock 10

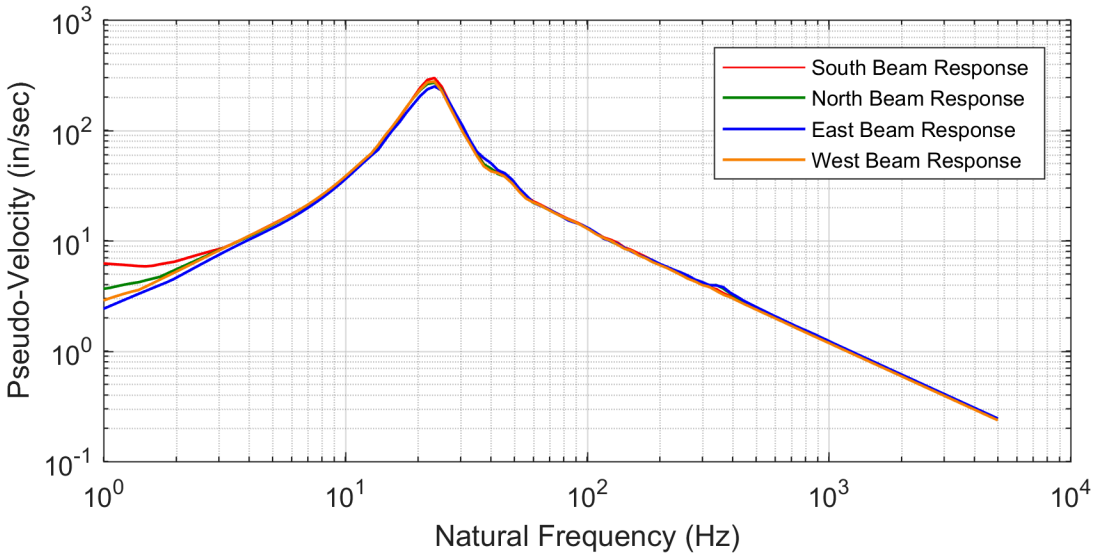

Figure 15. Pseudo-Velocity SRS from Accelerometers Mounted at Beam Tips—Shock 10

Figure 16 shows a plot of how the fundamental natural frequency of the individual cantilever beams shifted with the number of shocks applied. Since the testing was performed starting with pristine specimens and applying shocks until failure, this represents a measure of crack or damage growth within a cantilever beam structure. The beam on the fixture's South side failed first, followed by the beam on the West side, the North side, and finally, the East side beam failed. It is assumed that the step-wise decrease in the natural frequency corresponds to points of crack growth. It is not known if the crack growth was truly in discrete events or if the steps are largely due to the frequency resolution of the Fast Fourier Transform (FFT) used to obtain the beam frequency at each shock.

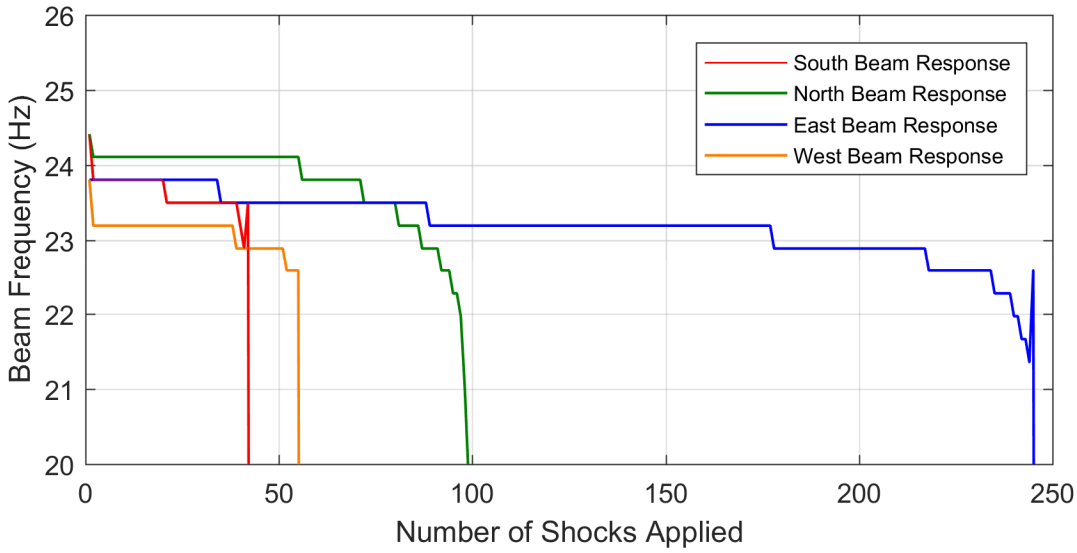

Figure 16. Change in Fundamental Beam Frequency with Number of Applied Shocks

Since time history data were collected at the free end of each cantilever beam, temporal moments were calculated for each beam at each shock event. The input shock was common for all four beams and the responses, as shown in Figure 14, were similar although some differences are apparent. To calculate the temporal moments for this analysis,

a common record length approach was used for all calculations. This eliminated the problem of correctly cropping each shock pulse for each beam. By using a fixed time window, the calculations are consistent across all shock events, even if the analyzed time window is not optimal.

Figure 17 shows a plot of the zeroth temporal moment, energy, with respect to the number of shocks applied for the four beams tested here. Comparing this plot with the beam frequency plot from Figure 16 shows a direct correlation between the beam failure order and the zeroth temporal moment. The South beam had the highest energy initially and it failed first. Interestingly enough, the energy level measured in the West beam, the second highest energy level, increased when the first beam failed. Likewise, when the second beam failed, the third beam energy level also increased. The final beam to fail did not show the jumps as the other beams failed but it does show a steady increase in energy as the other beams deteriorate and drop off.

While some definite differences were seen in the time histories between the four beam responses in Figure 14, the effects of the differences are difficult to quantify. The SRS, Figure 15, from the four beams are nearly identical and yield no obvious clues to the interaction between the four beams. However, the zeroth temporal moment shows immediately that the energy is not equally distributed. Furthermore, the fact that the energy redistributes among the remaining beams as beams are removed is a strong indication of the interplay present between the test specimens. Furthermore, it is most interesting to see, for example, that when the first beam failed, the energy does not evenly distribute to the other test beams but rather in this example was concentrated in what became the second beam to fail.

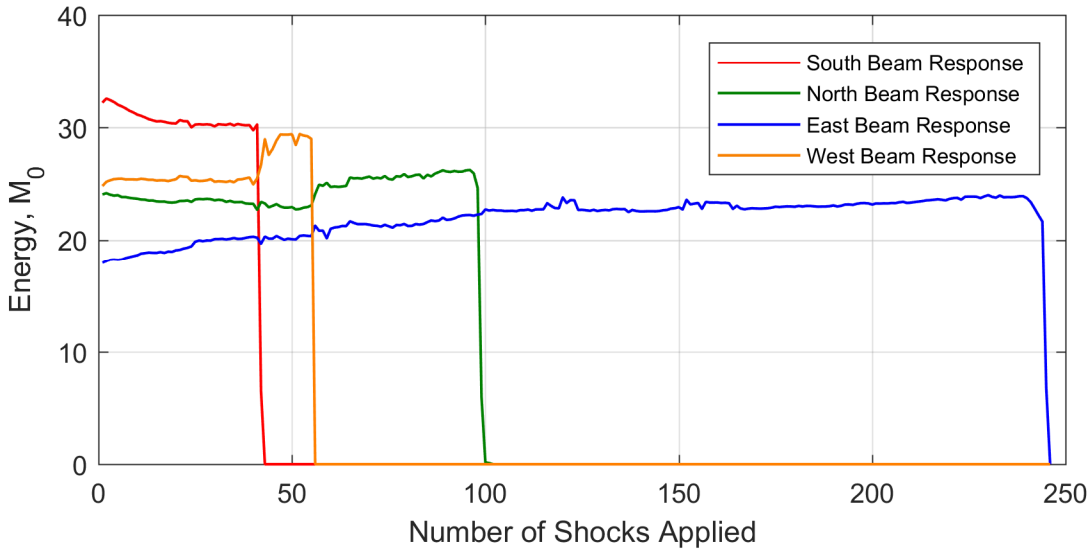

Figure 17. Changes in Shock Energy with Number of Applied Shocks

Figure 18 shows a similar trend with the calculated shock centroid. The shock centroid is the first temporal moment normalized by the zeroth temporal moment. It does not have the same significance as the energy or the RMS duration but it does indicate the location in time that approximately corresponds to the mid-point of the energy. As such, the further out in time the centroid is located, it can be assumed by extension that the shock pulse is longer for that component resulting in more applied energy. Here again, the results are the same as for the energy. The first beam to fail had the largest shock centroid, followed in order by the remaining three beams. It is also readily apparent in this plot that the responses adjust immediately but not necessarily equally to compensate for the loss of one component in the system. Again, indicating a strong presence of interplay between the components under test.

Figure 19 shows a plot comparing the RMS durations of the shock events for the four beams. While this plot is not as conclusive as the energy and shock centroid plots, it is nevertheless a strong indicator of the energy distribution between the four components. The outlier in Figure 19 is the North location beam which failed third in the series but

started out with an RMS duration nearly equal to the RMS duration of the first beam to fail and greater than the second beam to fail. The RMS duration of this beam eventually dropped below the RMS duration of the final beam to fail around shock 34 and did not return above that level until about the time that the first beam failed at shock 43. However, the RMS duration is not a true measure of the shock pulse duration, but rather a measure of the time on either side of the shock centroid which encompasses the bulk of the energy. Therefore, a short, high-energy shock will have a shorter RMS duration but may still contain more energy than a long, low-energy shock with a longer RMS duration. Thus, the RMS duration is a measure of pulse width but not necessarily a measure of pulse severity.

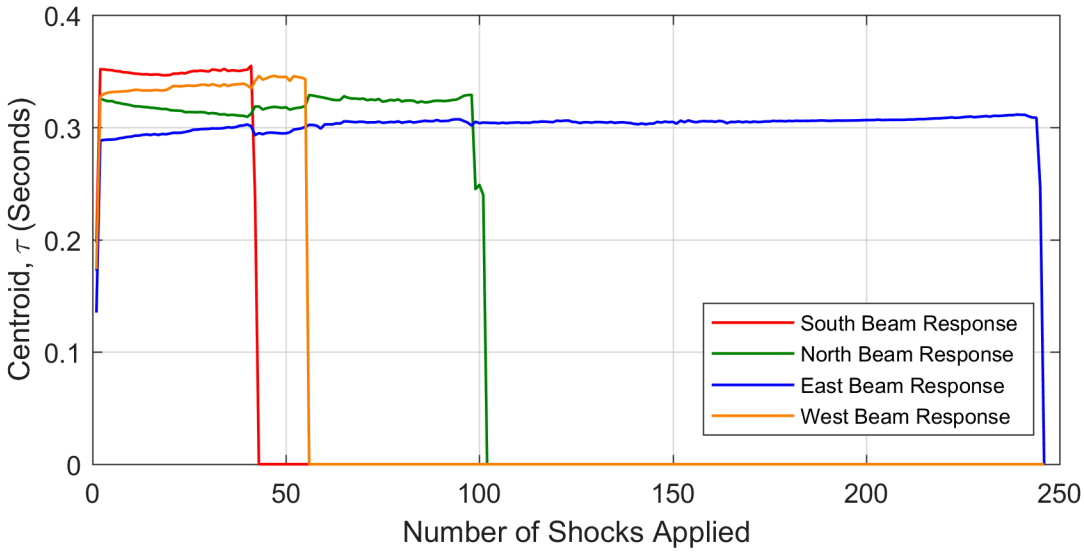

Figure 18. Changes in Shock Time History Centroid with Number of Applied Shocks

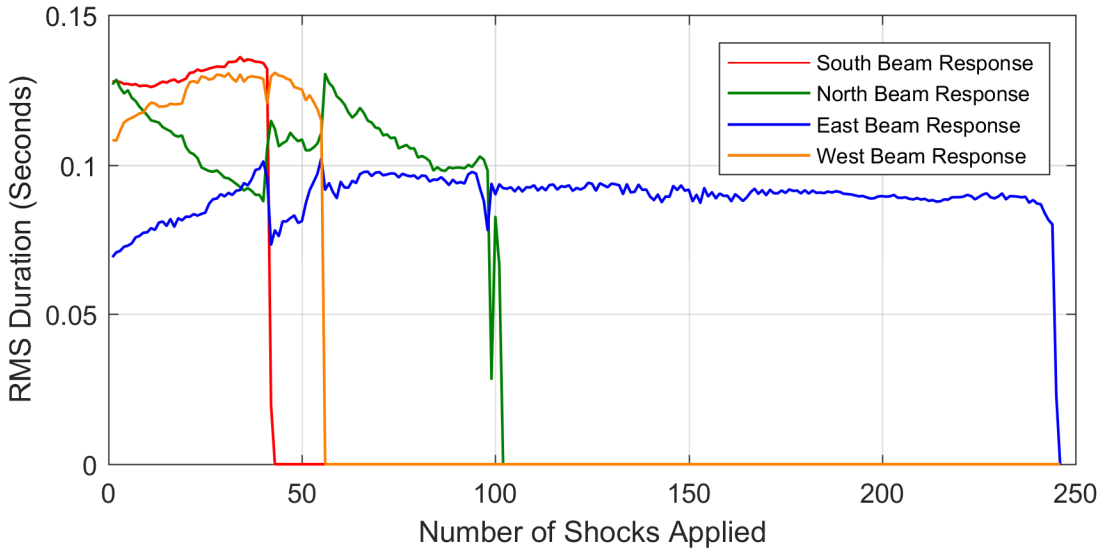

Figure 19. Changes in Shock RMS Duration with Number of Applied Shocks

Several sets of similar experiments were performed using new beams for each shock series. Figure 20 shows a plot of the zeroth temporal moment with respect to the number of applied shocks for four beams tested at a lower shock level. The shock input level here was approximately half of the shock acceleration used for the previous test series

and as a result, the number of shocks to failure was significantly greater. However, in both experiments, the South beam had the highest energy and failed first. The failure order for the remaining three beams is different from the previous test series but all still show the distinct changes in zeroth temporal moment as the beams fail. In this example, the first three beams failed in order of decreasing energy. The North beam had higher energy and lasted longer but this result could be attributed to unit-to-unit variability coupled with the lower input shock levels. Regardless, the beams still show distinct changes in response as the other beams fail, indicating that the temporal moments are detecting interplay between the various test specimen.

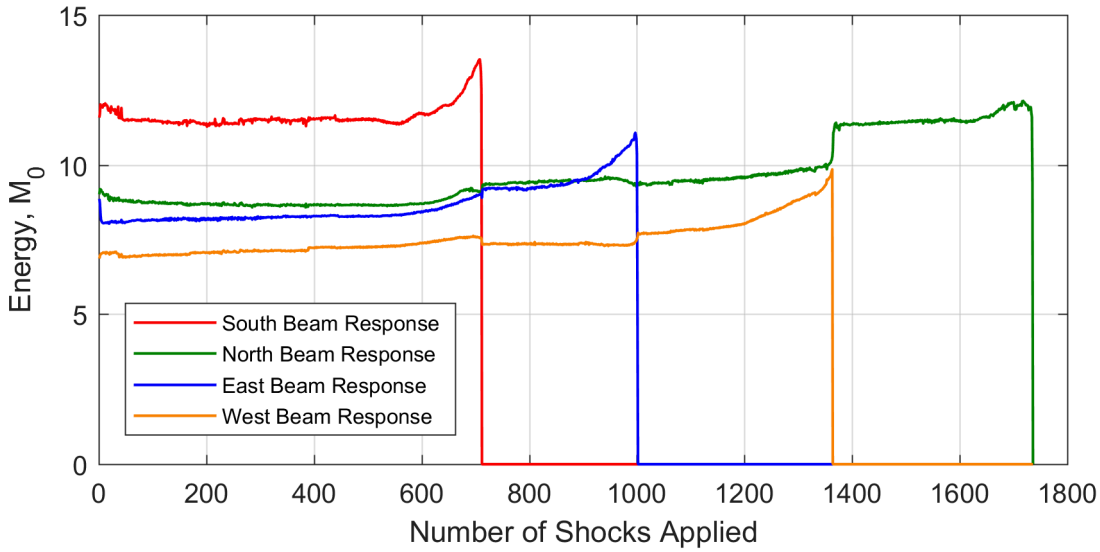

Figure 20. Changes in Shock Energy with Number of Applied Shocks for a Second Test Series Conducted at Lower Shock Energy Levels

CONCLUSION

Simultaneous testing of multiple identical components can often be a prudent use of laboratory test time and resources. However, it should be understood that there will be some interplay between components installed on a common test fixture. The interplay is a result of having closely spaced vibration modes resulting from multiple nominally identical components. The results presented here, from simultaneously testing four components, show that temporal moments do provide a good indicator of interplay between components on a common test fixture. The results also show that the responses are consistent across components and only change when the overall system changes, as with the failure of one component. As a result, temporal moments can be used to show that components assumed to be equally stressed in a shock test from SRS or peak acceleration response data actually have dissimilar responses.

REFERENCES

1. Scavuzzo, R. J. and Pusey, H. C., *Naval Shock Analysis and Design*, SVM-17, The Shock and Vibration Information Analysis Center, Booz-Allen and Hamilton, Inc., Falls Church, Virginia, 2000.
2. Smallwood, D. O. "Characterization and Simulation of Transient Vibrations Using Band Limited Temporal Moments," *Shock and Vibration*, Vol. 1, No. 6, pp. 507-527, 1994.
3. Smallwood, D., O., "Characterizing Transient Vibrations Using Band Limited Moments," *Proceedings of the 60th Shock and Vibration Symposium*, Virginia Beach, Virginia, November 1989.
4. Blevins, R. D., *Formulas for Natural Frequency and Mode Shape*, Krieger Publishing Company, Malabar, Florida, 2001.